



Experimental Study of the Effect of Laser-Cutting Process Parameters on Heat Distribution and Cutting Edge Quality of Steel Sheets

Mahsa Mokhtarian^{1,2}, Aazam Ghassemi*^{1,2}

¹Department of Mechanical Engineering, Najafabad Branch, Islamic Azad University, Najafabad, Iran

²Modern Manufacturing Technologies Research Center, Najafabad Branch, Islamic Azad University, Najafabad, Iran

*Corresponding Author: Aazam Ghassemi a_ghassemi@pmc.iaun.ac.ir

(Manuscript Received --- 11 Mar. 2018; Revised --- 24 Jun. 2018; Accepted --- 16 Jul. 2018)

Abstract

This study aimed to evaluate Laser-cutting process of Mild Steel St37 sheets with two different thicknesses. In order to evaluate the quality of cutting edge and the depth of the area affected by the heat, several tests were conducted to determine the effect of parameters such as Laser power, Laser beam movement speed and pressure of axillary gas on the quality of cutting edge and the depth of the area affected by the heat. The results showed that three main parameters of Laser beam movement speed, the pressure of axillary gas and Laser power could affect surface roughness and depth of the area affected by the heat. The value for each of these main parameters should be optimized based on other parameters and in a predetermined range in order to reach optimal conditions and edge quality and to use the interaction of these parameters to determine the final optimal conditions.

Keywords: Laser-cutting, Steel sheet, Quality of cutting edge, heat affected zone, finite elements.

1- Introduction

Given the widespread use of hard metals in various industries such as turbine fins of aerospace industries, automobile industries and other such uses, Laser-cutting has become an important tool for machining of steel alloys and super alloys. Among the advantages of Laser-cutting are high cut quality, high precision, low cut width, feasibility, low cutting heat, possibility of cutting without a pattern, high speed and productivity of this method [1]. Given the advantages of Laser-cutting process for industrial uses, it become widely accepted for industrial and engineering use. This in turn meant that parameter optimization for

improving the quality of the process became more important. As a result, many studies attempted to use various theoretical and empirical methods to emphasize various parts of the process in order to improve the yield and reducing the limitations of Laser-cutting. Studies around the world attempted to use different empirical methods to reduce the limitation of Laser-cutting process [2-4]. To this end, other studies used numerical [5-8] and analytical [9-11] methods along with empirical methods in order to maximize the speed and minimize the error of this process. Some of these studies are described below.

In 1998, Ling Chen [12] carried out an empirical systematic investigation on the effect of gas composition on CO₂ Laser-cutting of steel sheets. There are several non-linear parameters affecting Laser-cutting process. In this study, changes in gas composition and gas pressure were selected as main parameters and the results showed that small changes in the gas composition could affect the equality of the cut. The gas compositions used in this study included oxygen, argon, nitrogen and helium. The final results indicated that high-purity oxygen is necessary for high quality cuts on steel sheets using CO₂ Laser. A small impurity (1.25%) in the oxygen can reduce cutting speed by 50%. Karatas et al. in 2006 [13] carried out a study CO₂ Laser-cutting on steel sheets in which the convergence location of Laser beam compared to the sheets and the thickness of the sheet affected cut formation. They also investigated the cut's width using comprehensive parametric studies. Scanning electron microscope (SEM) and optical microscope were used to investigate the cut's location and the results showed that the convergence location has a large effect on the size of the cut and reduces the maximum possible workable thickness. The relative convergence location of the laser differs for different beams and cut widths.

Wasdara and Kojanpa in 2010 [14] investigated the yield of laser cutting process. They found out that the yield of laser cutting process is affected by melting rate and the rate of molten metal removal from the cut. The rate of flow and pleat removal from the cut depends on the yield of molten metal removal process and can be used to describe the rate of molten metal removal from the cut. Altovani et al.

[15] in another study investigated the CO₂ laser cutting process on class AISI 316L medical stainless steel. They used Box-Behnken experimental design method and empirical tests to optimize process parameters with emphasis on reducing process costs. To this end, parameters such as upper cut, lower cut, their ratio, cut roughness and process costs were selected as the factors affecting the equality of cut and a mathematical model was created between these factors and parameters of cut's quality. Finally, they proposed an optimum cutting condition for stainless steel with maximum quality and minimum process cost. Raoul et al. in 2017 [16] investigated laser cutting process of CFRP composite sheets. In this study, they used surface optimization method to determine optimum parameters. Parameters such as laser power, laser movement speed and axillary gas flow rate were selected as the most important process parameters with their optimum values were determined to be 260W laser power, 4500 mm/min speed and 14.23 for axillary gas flow for best quality with minimum surface deformations. Madik et al. [17] determined the parameters of laser cutting process using PCI technique. In this study, they performed an optimization of laser cutting process with the goal of proposing a novel multivariable decision-making method. They used dependent parameters of surface roughness, head affected area and machining rate as their output parameters and found out that this optimization method fully accurate and applicable if the values of input parameters are too close to each other. They found out that high concentration of laser beam at the cut's location and using maximum possible axillary gas pressure means that the cut will be free of any precipitations. Anjadi et

al. in 2017 [18] investigated the head affected area after laser cutting process on thin pure titanium sheets. They carried out several experiments using CO2 laser and L16 perpendicular array experimental design. The parameters investigated in their study included axillary gas pressure, distance between laser tip and the sheet, laser movement speed and laser power. After investigating the metallography and microstructures of the experimental samples, they found out that in laser cutting of titanium sheets, the speed must be as high as possible while the necessary energy is produced by changing the laser's power. Using helium instead of argon as the axillary gas can also help reduce the width of the cut.

The current study aims to investigate the laser cutting process of Mild Steel St37 sheets with two different thicknesses. In order to investigate the quality of the cutting edge and heat affected zone, several tests are carried out to determine the effects of parameters such as laser power, laser movement speed and axillary gas pressure on quality of cutting edge and depth of head affected area.

2- Experimental Studies

2.1- Sample Presentation

For sampling, cubic samples with minimum size of 5mm in each dimension were selected. In this study, sampling was carried out using ROBOFIL 200 wire-cutting equipment. Mounting includes placing the sample inside plastic materials which can be carried out using two cold and hot methods. This study used hot mounting method in which first sample is placed at the bottom of the mold on the side that should be investigated. Then the mounting powder is added to the mold. This powder is melted under pressure and

heat and surrounds the sample. Figure (1) shows a mounted sample used in this study. In the next stage, the mold is cooled using water or other cooling methods in order to prepare the mounted sample. The temperature necessary for melting the powder is 160°C.

In order to prepare the sample's surface, sanding, polishing and etching processes are carried out on the sample. Mounted samples are sanded using a size 60 sanding paper mounted on a rotating disk in order to remove surface unevenness. The main sanding process, we carried out in six stages using size 180, 240, 320, 600 and 1000 sanding paper with 180 being the roughest and 1000 being the softest paper. During the sanding process, constant water flow is present on the disks to remove the parts separated from the samples and produce a polished surface. Water flow also reduces the temperature created due to friction. Figure (2a) shows the disk sanding equipment used in this study. Polishing process is carried out to remove all remaining deformations on the surface. This process is carried out using a disk covered in Hairbrush or felt covered with a very soft abrasive material (such as aluminum or magnesium oxide). Hairbrush or felt used in this process must be thick and free of all hard particles such as dust which can cause scratches on the sample's surface. Figure (2b) shows the equipment used in polishing. Etching is the process of corroding metal's surface using a usually acidic solution. The etch solution used in this study is Nital 3% (3mL of HNO₃ and 100mL of ethanol).



Fig. 1, Mounted Samples Used in This Study



Fig. 2, (a) Sanding Equipment with Constant Water Flow, (b) Polishing Equipment Using in This Study.

2.2- Laser Cutting Equipment

A Carbon dioxide laser cutting equipment type Bystronic Bystar-4025 with maximum output power of 4.2KW was used for preparing the samples. Figure (3) shows the laser cutting equipment used in this study.



Fig. 3, (a) Bystronic Bystar-4025 Laser Cutting Equipment (b) Laser Cutting Equipment During Operation

2.3- Measurement Tools

For microscopic study of samples and observing their grain structure after etching and determining the quality of cutting edge, an OLYMPUS-SZ60 optical microscope and an OLYMPOUS-SZX16 stereomicroscope were used. In this study, surface roughness was measured using portable Time (TR200) equipment. Surface roughness measurement was carried out

three times and the average of the results is reported as the surface roughness. The equipment's probe moves on the samples' surface for the predetermined distance but due to difference in acceleration at the start and end of the movement, roughness measurement is not carried out at the start and end.

In order to measure the temperature during laser cutting process for evaluating the proposed finite element model, a thermocouple was used. This thermocouple is used to measure the temperature as predetermined locations and can measure temperatures up to 1000 degree Celsius. Since melting point of samples during cutting is higher than this temperature, it is not possible to place the thermocouple directly at the laser's path. Therefore, thermocouple is placed at a 2mm distance from cutting path using thermal glue in order to determine the temperature at laser's path. The thermocouple used is a fixable (spring-type) type-K thermocouple made in Korea with the length of 10cm and tip thickness of 1mm. It's working range is between 40 to 1060°C with precision of $\pm 1^\circ\text{C}$. Figure (4) shows the thermocouple used in this study. An ADVANTECH USB 4718 thermal module was used to extract and store thermal data.

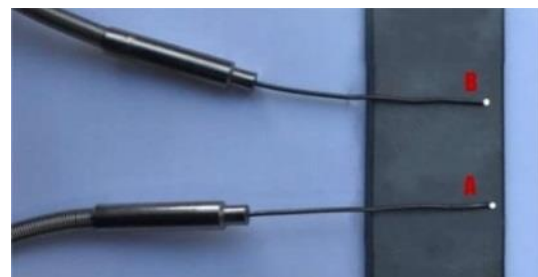


Fig. 4, The Location of Thermocouple on Sheet's Surface

2.4- Experiment Design

In this study, response surface method was used for modeling and prediction of the

results. Response surface method can also determine the interactions between two or more parameters and controllable input parameters [19]. When all independent variables are measurable with negligible error, response surface method has the form shown in (1):

$$y = f(x_1, x_2, x_3, \dots, x_k) \tag{1}$$

Which includes k independent variables. It is then necessary to determining the function between each independent variable and responses. Generally, a Quadratic polynomial similar to (2) is used in RSM for defining the model:

$$y = \beta_0 + \sum_{i=1}^k \beta_i x_i + \sum_{i=1}^k \beta_{ii} x_i^2 + \sum_i \sum_j \beta_{ij} x_i x_j + \varepsilon \tag{2}$$

In which ε is the expanded regression error. These experiments are designed based on the cube centric of REM [20]. Laser power, laser movement speed and axillary gas pressure are the independent input variables and Ra, Rz and depth of heat affected zone are selected as output variables. Figure (5) shows the Ra and Rz roughness variables.

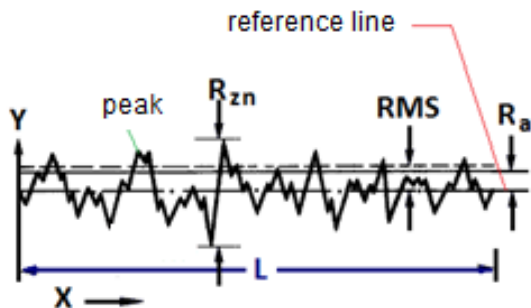


Fig. 5, Determination of Surface Roughness Parameters [21]

Surface roughness or profile, Ra, is a quantitative method for measuring

roughness. Ra is determined by linear measurement of roughness on the entire surface. There are various methods for measuring surface roughness which can be divided into contact and non-contact techniques. In contact techniques, which is the basis of profilometer equipment, surface roughness is measured by moving a sensor tip on the surface. Electron microscope is a common method of non-contact measurement of surface roughness. After measuring surface roughness profile, its relative ratio is reported using industrial standard measures. Ra surface roughness profile is usually seen as increasing and decreasing peaks measured against a baseline. Ra value is determined using (3):

$$Ra = \frac{1}{L} \int_0^L |Y(x)| dx \tag{3}$$

Ten-point average roughness, Rz, is a parameter replacing surface roughness profile which is determined through perpendicular measurement of five points with highest peaks and five of the lowest indents, using the average of these ten measurements as surface roughness using (4):

$$Rz = \frac{1}{5} (R_{z1} + R_{z2} + R_{z3} + R_{z4} + R_{z5}) \tag{4}$$

In this study, the main goal is to investigate laser cutting on Mild Steel St37 sheets with thickness of 4 and 6mm. Table (1) shows the designed experiments based on cubic centric design. By adding the values for power, speed and gas pressure parameters, experiments are carried out according to tables (2) and (3).

Table 1- Experiments Designed Based on Cubic Centric Design (CCD)

| P (bar) | V (m/min) | Power (W) |
|---------|-----------|-----------|
| -1 | -1 | -1 |
| -1 | -1 | 1 |
| -1 | 1 | -1 |
| -1 | 1 | 1 |
| 1 | -1 | -1 |
| 1 | -1 | 1 |
| 1 | 1 | -1 |
| 1 | 1 | 1 |
| 0 | 0 | -2 |
| 0 | 0 | 2 |
| 0 | -2 | 0 |
| 0 | 2 | 0 |
| 2 | 0 | 0 |
| 2 | 0 | 0 |
| 0 | 0 | 0 |
| 0 | 0 | 0 |
| 0 | 0 | 0 |
| 0 | 0 | 0 |
| 0 | 0 | 0 |
| 0 | 0 | 0 |
| 0 | 0 | 0 |
| 0 | 0 | 0 |

Table 2- Experiment Design Using Response Surface Method (RSM) with Actual Parameter Values for Mild Steel St37 Sheet with 4mm of Thickness

| P (bar) | V (m/min) | Power (W) |
|---------|-----------|-----------|
| 2 | 1 | 1000 |
| 2 | 1 | 2000 |
| 2 | 2 | 1000 |
| 2 | 2 | 2000 |
| 3 | 1 | 1000 |
| 3 | 1 | 2000 |
| 3 | 2 | 1000 |
| 3 | 2 | 2000 |
| 2.5 | 1.5 | 500 |
| 2.5 | 1.5 | 2500 |
| 2.5 | 1 | 1500 |
| 2.5 | 2.5 | 1500 |
| 1.5 | 0.5 | 1500 |
| 3.5 | 1.5 | 1500 |
| 2.5 | 1.5 | 1500 |
| 2.5 | 1.5 | 1500 |
| 2.5 | 1.5 | 1500 |
| 2.5 | 1.5 | 1500 |
| 2.5 | 1.5 | 1500 |

Table 3- Experiment Design Using Response Surface Method (RSM) with Actual Parameter Values for Mild Steel St37 Sheet with 4mm of Thickness

| P (bar) | V (m/min) | Power (W) |
|---------|-----------|-----------|
| 2 | 1 | 1000 |
| 2 | 1 | 2000 |
| 2 | 2 | 1000 |
| 2 | 2 | 2000 |
| 3 | 1 | 1000 |
| 3 | 1 | 2000 |
| 3 | 2 | 1000 |
| 3 | 2 | 2000 |
| 2.5 | 1.5 | 500 |
| 2.5 | 1.5 | 2500 |
| 2.5 | 1 | 1500 |
| 2.5 | 2.5 | 1500 |
| 1.5 | 0.5 | 1500 |
| 3.5 | 1.5 | 1500 |
| 2.5 | 1.5 | 1500 |
| 2.5 | 1.5 | 1500 |
| 2.5 | 1.5 | 1500 |
| 2.5 | 1.5 | 1500 |
| 2.5 | 1.5 | 1500 |
| 2.5 | 1.5 | 1500 |
| 2.5 | 1.5 | 1500 |

3- Finite Element Analysis for Laser-Cutting

In this section, the thermal behavior of samples during laser cutting process is simulated using finite element analysis with the help of ABAQUS software package. To this end, a three-dimensional non-linear thermal transient model is created. In the direct line heating process, laser beam moves along a straight line and heats the sheet, which melts the sample. Parameters of laser cutting process and their values used in this simulation are shown in table (4).

Table 4- Parameters Used for Process Simulation

| Laser parameters | | Work piece parameters | |
|------------------|-----------------------------------|-----------------------|---------------|
| 500 ~ 2500 | Power(W) | 4 ~ 6 | Thickness(mm) |
| 0.2 | Beam (mm) diameter | 20 | Length(mm) |
| 0.5 ~ 2.5 | Beam ($\frac{m}{min}$) velocity | 20 | Width(mm) |

3.1- Modeling of Sample

The sample was modeled with dimensions of 20x20mm with two different thicknesses of 4 and 6mm in ABAQUS software. Since laser cutting process has a high thermal flow, the thermal characteristics of the material change, leading to different behaviors. Therefore, the time dependence of thermal characteristics such as specific thermal capacity, thermal conductivity coefficient and other similar parameters should be considered and these parameters must be modeled as functions of temperature [22]. In this study, transient heat technique was for finite element analysis of laser cutting process. Heat loss on the sheet is due to convection and radiation of heat to the surrounding environment. Convection heat loss is calculated using (5) [23].

$$q_c = h_f(T_s - T_\infty) \quad (5)$$

In which h_f is convection heat transfer coefficient, T_s is temperature at sheet's surface, T_∞ is the outside temperature and q_c is the heat loss due to convection.

Radiation heat loss is calculated using (6) [24].

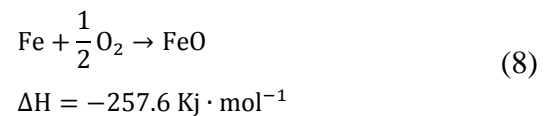
$$q_r = \sigma \varepsilon_r (T_s^4 - T_\infty^4) \quad (6)$$

In which σ is Boltzmann constant, ε_r is the surface radiation coefficient, T_s is temperature at sheet's surface, T_∞ is the outside temperature and q_r is heat loss due to radiation. The process is carried out under normal conditions and therefore convection heat transfer coefficient of air is 200W/m²C, radiation coefficient is 0.7 and outside temperature is 25°C.

Heat distribution in an object in three-dimensional form is calculated using law of conservation of thermal energy (7) [23].

$$\rho C_p \frac{\partial T}{\partial t} = \frac{\partial}{\partial x} \left(k \frac{\partial T}{\partial x} \right) + \frac{\partial}{\partial y} \left(k \frac{\partial T}{\partial y} \right) + \frac{\partial}{\partial z} \left(k \frac{\partial T}{\partial z} \right) + q_{\text{heat}} \quad (7)$$

In which k is thermal conductivity coefficient, t is the time, T is the temperature, ρ is the density of the material, q is the heat source, and CP is specific heat capacity at constant pressure. Border conditions for the edge of laser cut is $\frac{\partial T}{\partial x} = 0$ in a symmetrical plane and $-k \frac{\partial T}{\partial n} = \alpha_T (T - T_\infty)$ in other planes in which T_∞ is the outside temperature and α_T is the combined heat transfer coefficient. It is necessary to mention that during laser cutting process, other than the heat due to laser beam, another term is added to the total heat (heat flow) which is due to exothermic oxidation reaction of steel [25]. Equation (8) shows the exothermic oxidation reaction of steel.



Therefore, in finite element simulation, other than heat flow to the sample which has a Gaussian distribution, the heat of the oxidation reaction is also considered. Equation (9) shows the heat flow in the simulated process.

$$Q(x, y, z) = Q_0 e^{-\frac{x^2+y^2}{r^2}} + \frac{\Delta H}{\left(h \cdot \frac{\pi d_0^2}{4} \right)} ; \quad (9)$$

$$Q_0 = \frac{\alpha P}{\left(h \cdot \pi d_0^2 / 4 \right)}$$

In which α is the adsorption coefficient and ΔH is the energy of exothermic reaction; r is the radius of laser beam, Q_0 is the actual energy compression and Q is the density of

heat flow. For meshing of the model, a heterogeneous pattern is used so that a smaller mesh is used at the path of laser beam. As seen in figure (6), locations further away from the laser beam's path have larger mesh size which is due to decreased heat transfer rate at these locations.

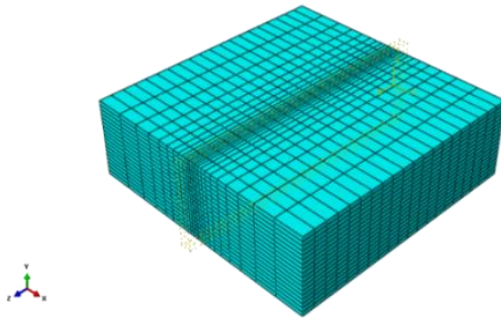
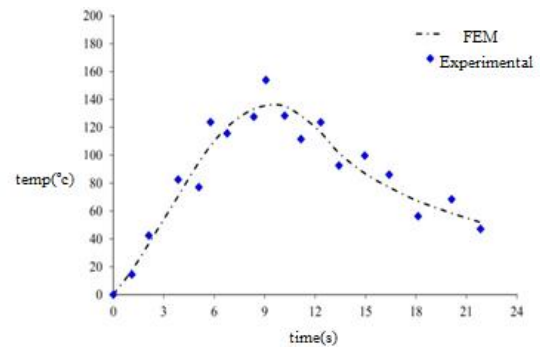


Fig. 6, Meshing Pattern Used in Simulation Process.

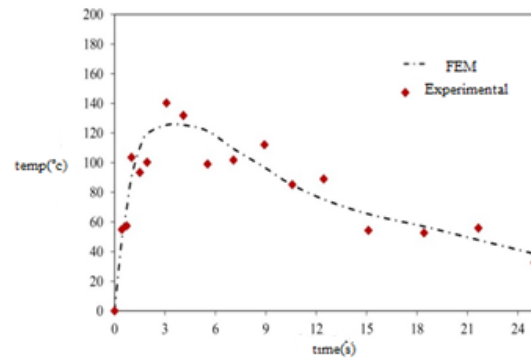
3.2- Evaluation of Finite Element Simulation of Laser Cutting Process

In this study, simulation results are evaluated by comparing them to the empirical results. To this end, using a thermocouple, the temperature of the sample with the thickness of 4mm is measured at two different points and compared with the results of the simulation. Figure (7) shows the changes of temperature in these thermocouples which are placed 2mm away from laser's path and at the distance of 5 and 15mm from the start of the cutting process. The speed of the beam is 1m/min, laser power is 1000W and gas pressure is 2barr. As can be seen in figure (7), the results obtained from finite element analysis manage to determine the temperatures of the determined points (the location of thermocouples) with acceptable error. The existing difference is probably due to assumptions and simplifications in the numerical (finite element) analysis. Now, finite element analysis can be used to investigate the depth of heat affected zone

and changing the parameters under different conditions can be used to determine the optimal (minimum) depth of heath affected area under optimal process parameters. This helps reduce the number of experiments necessary for empirical determination of parameters for reaching optimal depth of heat affected zone (considering each parameter and their interactions) and thus save time and reduce the cost of experiments.



(a)



(b)

Fig. 7, (a) The Temperature Comparison at the Location of Thermocouple A, (b) Temperature Changes at Point B (Second Thermocouple) in Experimental and Numerical Studies.

4- General Results and Discussions

4.1- The Depth of Heat Affected Zone

In order to investigate the depth of heat affected zone, in simulations, each sample is cut using a plane parallel to x-y axis as shown in figure (8) in order to determine the depth of heat affected zone. The depth of heat affected zone in sheets with depth of 4 and 6mm can be seen in figures (9)

and (10) respectively. The heat produced during laser cutting process greatly affects steel microstructures in the heat affected zone. The results of the experiments clearly show this area and changes in grain size. The upper part of figure (11) which has a lighter color is the center of the sample and has a ferrite perlite structure. By moving from the center of the sample toward the heat affected zone, structure changes to Martensite and needle-like grains. The depth of heat affected zone under conditions of 2000W power, movement speed of 1m/min and axillary gas pressure of 2barr s between 0.15 to 0.2mm. Table (5) shows the results of simulation n ABAQUS software and their comparison with experimental results.

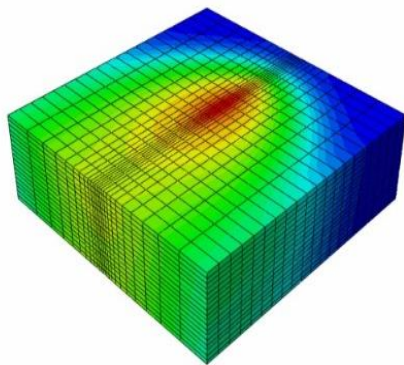
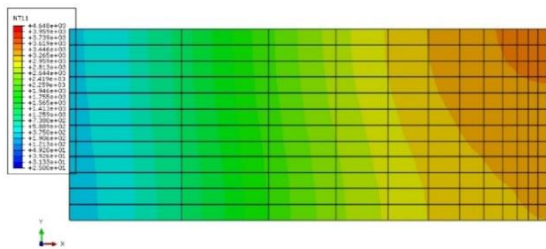
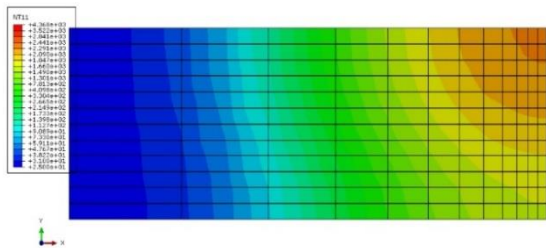


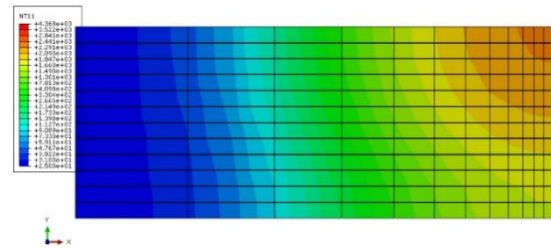
Fig. 8, Three-Dimensional Modeling of Laser Movement on the Sheet’s Surface



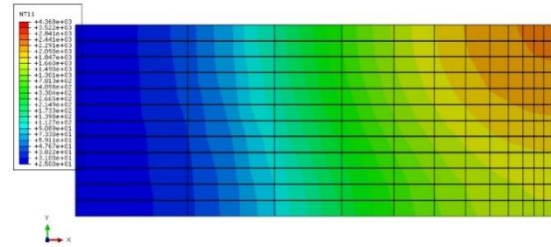
(a)



(b)

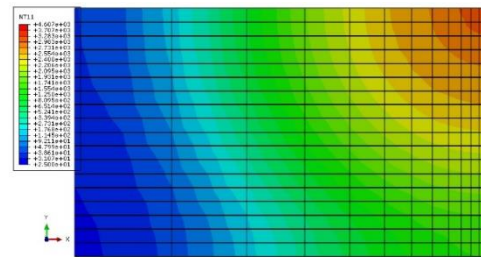


(c)

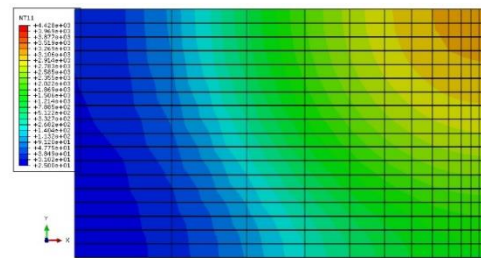


(d)

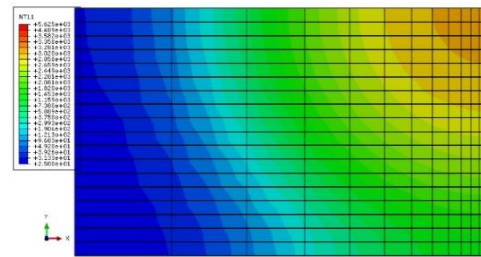
Fig. 9, Depth of Heat Affected Zone in the Sheet with Thickness of 4mm by Considering 3 Elements in Each Millimeter of the Sheet (a) Power 1500W and Speed of 0.5m/min, (b) Power of 1500W and Speed of 1m/min, (c) Power of 2000W and Speed of 1m/min and (d) Power of 1000W and Speed of 1m/min



(a)



(b)



(c)

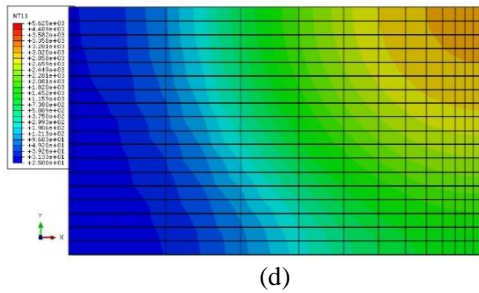


Fig. 10, Depth of Heat Affected Zone in the Sheet with Thickness of 6mm by Considering 3 Elements in Each Millimeter of the Sheet (a) Power 1500W and Speed of 0.5m/min, (b) Power of 1500W and Speed of 1m/min, (c) Power of 2000W and Speed of 1m/min and (d) Power of 1000W and Speed of 1m/min

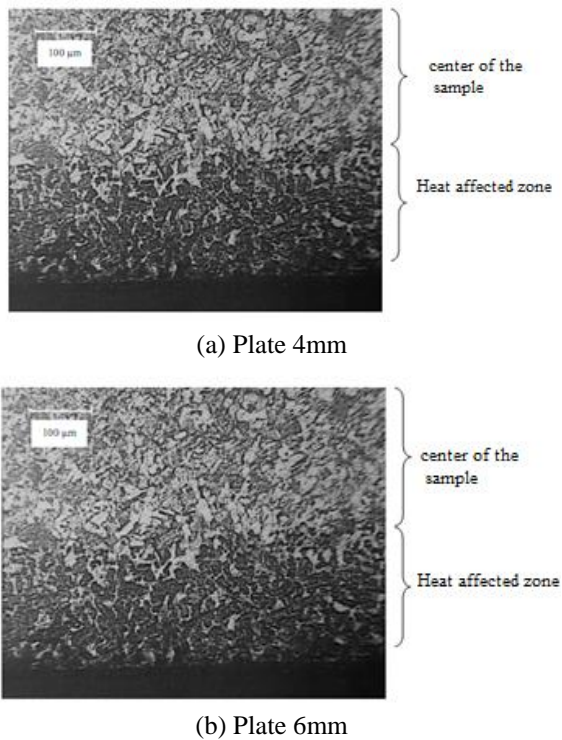


Fig. 11, Metallography of the Cut Sheets Using 2000W Power, Movement Speed of 1m/min and Axillary Gas Pressure of 2 bar

4.2 Surface Roughness Evaluation in Sheets with Thickness of 4 and 6 mm Using Empirical Method

After carrying out the experiments indicated using response surface method, data presented in tables 6 and 7 were extracted for sheets with thickness of 4 and 6mm respectively. The regression equations for evaluating the surface

roughness for sheets with thickness of 4 and 6mm are seen in (10) and (11) respectively.

$$\begin{aligned}
 Ra = & -0.00887443 \\
 & -1.49193(\text{speed}) \\
 & -15.1924(\text{pre}) + 4.42273E \\
 & -06(\text{pow})^2 \\
 & + 1.86773(\text{speed})^2 \\
 & + 3.20273(\text{pre})^2 - 0.00228500 \\
 & (\text{pow} \times \text{speed}) + 26.6351
 \end{aligned} \quad (10)$$

$$\begin{aligned}
 Ra = & -0.00146989 (\text{pow}) \\
 & -9.08739(\text{speed}) \\
 & -16.2065(\text{pre}) \\
 & + 2.25955E - 06(\text{pow})^2 \\
 & + 4.91955(\text{speed})^2 + 3.42955(\text{pre})^2 \\
 & - 0.00306500(\text{pow} \\
 & \times \text{speed}) + 29.5855
 \end{aligned} \quad (11)$$

After determining the regression equations for evaluation of surface roughness, the relation between input and output parameters were investigated. According to the speed – pressure graphs shown in figures (12) and (13), increase in cutting speed at a constant gas pressure first decreases the surface roughness and then the roughness increases after cutting speed exceeds 2m/min. Therefore, it can be concluded that by increasing the speed after a certain point, the rate of energy transfer to the sample in units of time decreases which in turn decreases the temperature from the temperature necessary for proper melting and removal of molten metal, thus increasing the surface roughness. Increase in axillary gas pressure also decreases the roughness at first but sharply increases the surface roughness after a certain point which indicates the large effect of axillary gas pressure on surface roughness. As can be seen in figures (14) and (15), the power –

pressure graphs also show that both parameters should be in an optimal range. Selecting values lower or higher than the optimal values for each parameter can lead to sharp increase in surface roughness. The power – speed graphs presented in figures (16) and (17) show that at low power levels (600W), increase in speed sharply increases the surface roughness which is due to lack of sufficient temperature for melting the metal at the beam's contact point. This effect is somewhat lessened with increase in the laser's power output until the roughness reaches its minimum value. Any further increases in the power

also increases the surface roughness which is due to lower quality of the cut as a result of exceedingly high temperatures and splashing of molten metal and surface oxidation. The results also show that the process for thickness of 6mm is almost similar to that of 4mm thickness with the only difference being a generally higher surface roughness. In general, in laser cutting process, surface roughness increases with increase in sheet's thickness. The main reason for this is divergence of the laser beam at higher thicknesses and moving away from its focal point.

Table 5- Experiment Design Using Response Surface Method for Mild Steel St37 (a) with Thickness of 4mm and Roughness as Output, (b) Thickness of 6mm and Roughness as Output.

| (a) | | | | | (b) | | | | |
|------|-------|-----|------|-------|------|-------|-----|-------|-------|
| pow | speed | pre | Ra | Rz | pow | speed | pre | Ra | Rz |
| 1000 | 1 | 2 | 2.64 | 17.91 | 1000 | 1 | 2 | 4.26 | 22.31 |
| 2000 | 1 | 2 | 4.51 | 19.82 | 2000 | 1 | 2 | 6.78 | 30.54 |
| 1000 | 2 | 2 | 4.87 | 20.17 | 1000 | 2 | 2 | 6.81 | 29.81 |
| 2000 | 2 | 2 | 4.42 | 19.72 | 2000 | 2 | 2 | 6.32 | 27.38 |
| 1000 | 1 | 3 | 3.55 | 18.83 | 1000 | 1 | 3 | 5.38 | 24.38 |
| 2000 | 1 | 3 | 5.48 | 20.68 | 2000 | 1 | 3 | 7.58 | 35.38 |
| 1000 | 2 | 3 | 5.14 | 20.44 | 1000 | 2 | 3 | 7.84 | 36.28 |
| 2000 | 2 | 3 | 4.82 | 20.12 | 2000 | 2 | 3 | 6.92 | 36.62 |
| 500 | 1.5 | 2.5 | 5.46 | 20.66 | 500 | 1.5 | 2.5 | 5.68 | 25.68 |
| 2500 | 1.5 | 2.5 | 7.81 | 23.19 | 2500 | 1.5 | 2.5 | 6.87 | 31.76 |
| 1500 | 1 | 2.5 | 3.48 | 19.18 | 1500 | 1 | 2.5 | 7.76 | 36.86 |
| 1500 | 2.5 | 2.5 | 4.68 | 19.88 | 1500 | 2.5 | 2.5 | 10.11 | 41.15 |
| 1500 | 0.5 | 1.5 | 4.41 | 19.71 | 1500 | 0.5 | 1.5 | 6.45 | 28.45 |
| 1500 | 1.5 | 3.5 | 6.42 | 21.72 | 1500 | 1.5 | 3.5 | 8.44 | 38.46 |
| 1500 | 1.5 | 2.5 | 2.24 | 17.54 | 1500 | 1.5 | 2.5 | 4.02 | 21.05 |
| 1500 | 1.5 | 2.5 | 1.98 | 17.18 | 1500 | 1.5 | 2.5 | 3.58 | 19.68 |
| 1500 | 1.5 | 2.5 | 2.15 | 17.45 | 1500 | 1.5 | 2.5 | 3.98 | 22.18 |
| 1500 | 1.5 | 2.5 | 2.42 | 17.72 | 1500 | 1.5 | 2.5 | 4.12 | 24.26 |
| 1500 | 1.5 | 2.5 | 2.12 | 17.42 | 1500 | 1.5 | 2.5 | 3.88 | 22.38 |
| 1500 | 1.5 | 2.5 | 2.05 | 17.35 | 1500 | 1.5 | 2.5 | 4.15 | 24.66 |

Table 6- ANOVA Results for Ra in Mild Steel St37 with (a) Thickness of 4mm (b) Thickness of 6mm

| (a) | | | | | | |
|----------------|----|---------|---------|---------|--------|-------|
| Source | DF | Seq SS | Adj SS | Adj MS | F | P |
| Regression | 7 | 50.4896 | 50.4896 | 7.2128 | 117.61 | 0 |
| Linear | 3 | 8.3024 | 8.3024 | 2.7675 | 45.13 | 0 |
| pow | 1 | 3.7346 | 3.7346 | 3.7346 | 60.9 | 0 |
| speed | 1 | 1.8701 | 1.8701 | 1.8701 | 30.49 | 0 |
| pre | 1 | 2.6078 | 2.6978 | 2.6978 | 43.99 | 0 |
| Square | 3 | 39.5766 | 39.5766 | 13.1922 | 215.11 | 0 |
| pow*pow | 1 | 21.1588 | 30.738 | 30.738 | 501.21 | 0 |
| speed*speed | 1 | 2.2989 | 5.4818 | 5.4818 | 89.39 | 0 |
| pre*pre | 1 | 16.1189 | 16.1189 | 16.1189 | 262.83 | 0 |
| Interaction | 1 | 2.6106 | 2.6106 | 2.6106 | 42.57 | 0 |
| pow*speed | 1 | 2.6106 | 2.6106 | 2.6106 | 42.57 | 0 |
| Residual Error | 12 | 0.7359 | 0.7359 | 0.0613 | | |
| Lack-of-Fit | 7 | 0.6157 | 0.6157 | 0.088 | 3.66 | 0.086 |
| Pure Error | 5 | 0.1202 | 0.1202 | 0.024 | | |
| Total | 19 | 51.2256 | | | | |

| (b) | | | | | | |
|----------------|----|---------|---------|---------|--------|-------|
| Source | DF | Seq SS | Adj SS | Adj MS | F | P |
| Regression | 7 | 63.2517 | 63.2517 | 9.036 | 206.18 | 0 |
| Linear | 3 | 10.1791 | 10.1791 | 3.393 | 77.42 | 0 |
| pow | 1 | 2.0235 | 2.0235 | 2.0235 | 46.17 | 0 |
| speed | 1 | 4.6118 | 4.6118 | 4.6118 | 105.23 | 0 |
| pre | 1 | 3.5438 | 3.5438 | 3.5438 | 80.86 | 0 |
| Square | 3 | 48.3756 | 48.3756 | 16.1252 | 367.94 | 0 |
| pow*pow | 1 | 1.0507 | 8.023 | 8.023 | 183.06 | 0 |
| speed*speed | 1 | 28.842 | 38.0316 | 38.0316 | 867.78 | 0 |
| pre*pre | 1 | 18.4828 | 18.4828 | 18.4828 | 421.73 | 0 |
| Interaction | 1 | 4.6971 | 4.6971 | 4.6971 | 107.18 | 0 |
| pow*speed | 1 | 4.6971 | 4.6971 | 4.6971 | 107.18 | 0 |
| Residual Error | 12 | 0.5259 | 0.5259 | 0.0438 | | |
| Lack-of-Fit | 7 | 0.3096 | 0.3096 | 0.0442 | 1.02 | 0.509 |
| Pure Error | 5 | 0.2163 | 0.2163 | 0.0433 | | |
| Total | 19 | 63.7777 | | | | |

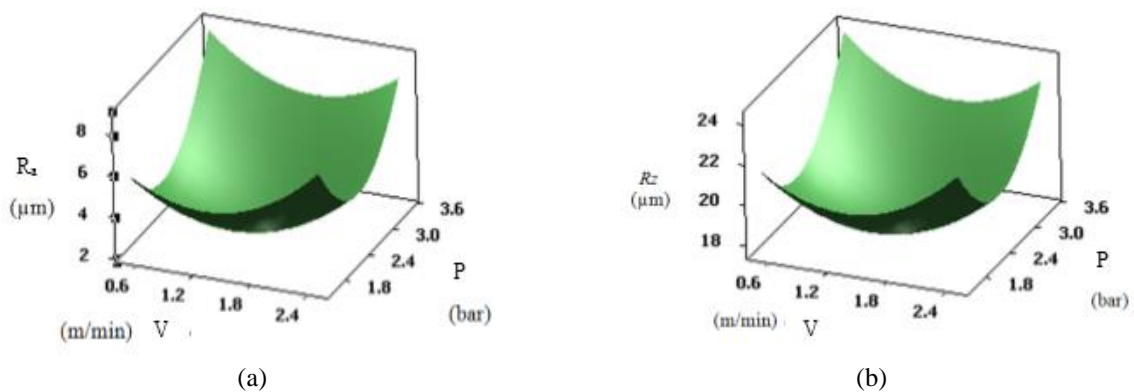
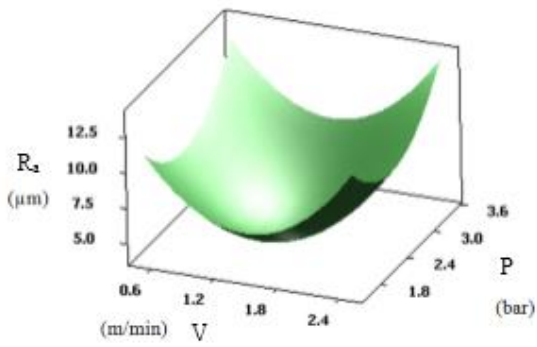
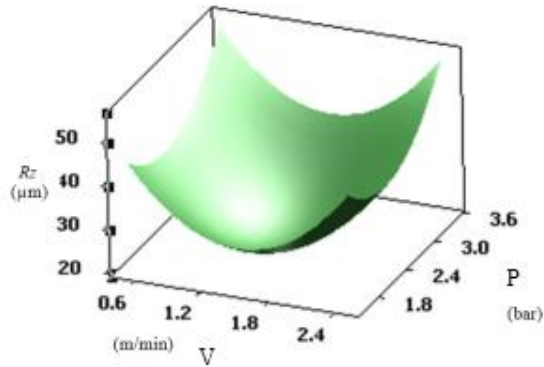


Fig. 12- The Effect of Axillary Gas Pressure and Cutting Speed on (a) Average Surface Roughness Ra and (b) Rz in 4mm Sheet at the Power of 1700W

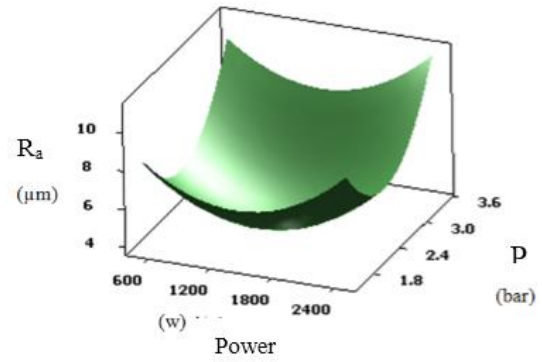


(a)

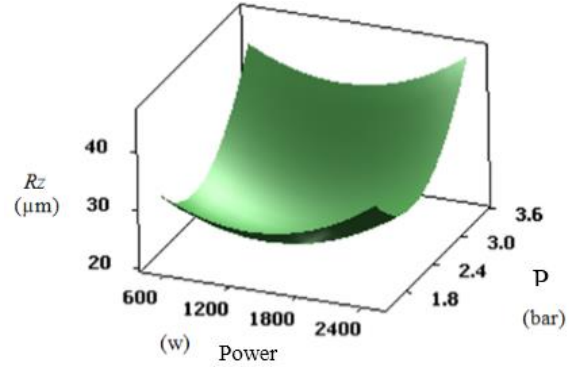


(b)

Fig 13- The Effect of Axillary Gas Pressure and Power on (a) Average Surface Roughness Ra and (b) Rz in 4mm Sheet at the Power of 1700W

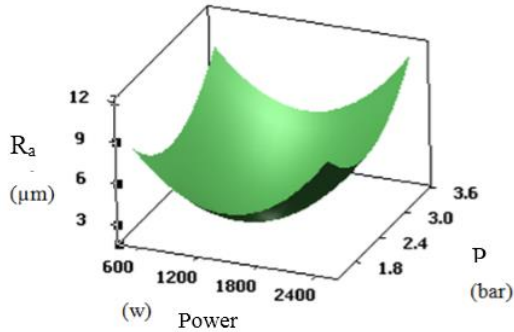


(a)

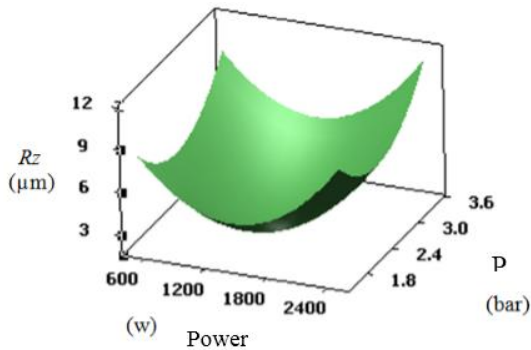


(b)

Fig. 15- The Effect of Axillary Gas Pressure and Laser Power on (a) Average Surface Roughness Ra and (b) Rz in 6mm Sheet with the Cutting Speed of 1.6m/min

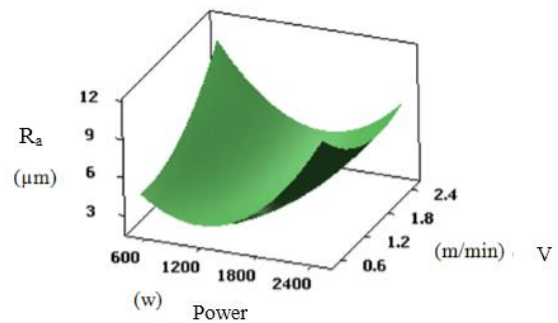


(a)

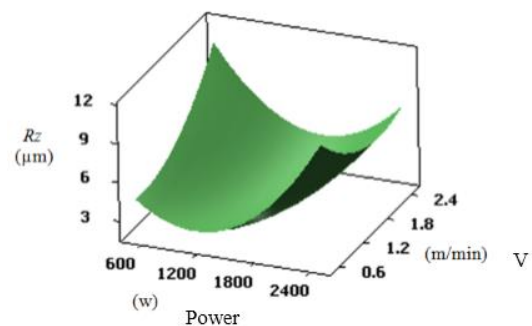


(b)

Fig. 14- The Effect of Axillary Gas Pressure and Laser Power on (a) Average Surface Roughness Ra and (b) Rz in 4mm Sheet with the Cutting Speed of 1.6m/min



(a)



(b)

Fig. 16- The Effect of Power and Cutting Speed Parameters on (a) Average Surface Roughness Ra and (b) Rz for 4mm Sheets at Axillary Gas Pressure of 2.5bar

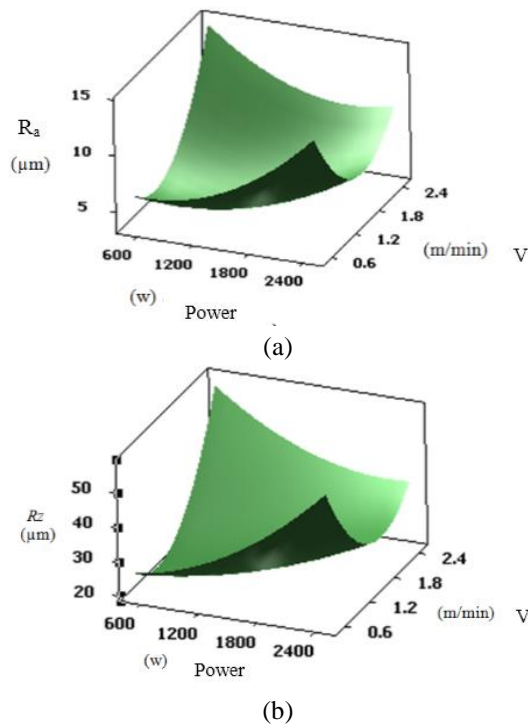


Fig. 17, The Effect of Power and Cutting Speed Parameters on (a) Average Surface Roughness R_a and (b) R_z for 6mm Sheets at Axillary Gas Pressure of 2.5bar

4.3- Evaluating the Depth of Heat Affected Zone (HAZ) IN 4mm Sheets

After carrying out the experiments designed based on response surface method, the responses for Mild Steel St37 sheet with thickness of 4mm were extracted and presented in tables (8) and (9). Regression equations for evaluating the depth of heat affected zone in the upper one-third and lower two-third of the thickness of 4mm sheets are presented in (12) and (13).

$$\begin{aligned} \text{HAZ} - 4 = & 0.0700000 (\text{pow}) \\ & - 31.0000(\text{speed}) \\ & - 71.0000(\text{pre}) \\ & + 15.5000(\text{speed})^2 \\ & + 10.5000(\text{pre})^2 \\ & - 0.0260000(\text{pow} \\ & \times \text{speed}) + 170.500 \end{aligned} \quad (12)$$

$$\begin{aligned} \text{HAZ} - 4D = & 0.0435000(\text{pow}) \\ & - 331.643(\text{speed}) \\ & - 112.571(\text{pre}) \\ & + 134.214(\text{speed})^2 \\ & + 29.2143(\text{pre})^2 \\ & + 353.286 \end{aligned} \quad (13)$$

Using these equations, it is possible to evaluate the relation between output and input parameters and their effect on the depth of HAZ in the upper one-third and lower two-third of the sheet's thickness. The power -speed graphs in figure (18) shows that, generally, with increase in laser power, the depth of HAZ increases. This effect is larger at lower speeds. The reason for this change is the change in the rate of heat transfer to the sample. Also, in lower cutting speeds, sample spends more time in contact with the laser beam, which in turn increases the rate of heat transfer and depth of HAZ.

Table 7- Experiment Design Using Response Surface Method for Mild Steel St37 Sheets with 4mm Thickness with HAZ Depth as the Output.

| power | speed | pre | D1.30 up/t=4 | D2.30 down/t=4 |
|-------|-------|-----|-----------------|-------------------|
| 1000 | 1 | 2 | 100 | 120 |
| 2000 | 1 | 2 | 150 | 160 |
| 1000 | 2 | 2 | 90 | 180 |
| 2000 | 2 | 2 | 120 | 180 |
| 1000 | 1 | 3 | 80 | 100 |
| 2000 | 1 | 3 | 150 | 180 |
| 1000 | 2 | 3 | 72 | 200 |
| 2000 | 2 | 3 | 90 | 278 |
| 500 | 1.5 | 2.5 | 70 | 80 |
| 2500 | 1.5 | 2.5 | 120 | 160 |
| 1500 | 1 | 2.5 | 130 | 180 |
| 1500 | 2.5 | 2.5 | 80 | 320 |
| 1500 | 0.5 | 1.5 | 120 | 180 |
| 1500 | 1.5 | 3.5 | 80 | 180 |
| 1500 | 1.5 | 2.5 | 90 | 120 |
| 1500 | 1.5 | 2.5 | 85 | 130 |
| 1500 | 1.5 | 2.5 | 90 | 125 |
| 1500 | 1.5 | 2.5 | 97 | 120 |
| 1500 | 1.5 | 2.5 | 80 | 115 |
| 1500 | 1.5 | 2.5 | 100 | 110 |

Table 8- ANOVA Results for HAZ-4 with (a) HAZ in Upper One-Third of 4mm Sheet (b) HAZ in Lower Two-Third of 4mm Sheet

| (a) | | | | | | |
|----------------|----|--------|--------|---------|-------|-------|
| Source | DF | Seq SS | Adj SS | Adj MS | F | P |
| Regression | 6 | 8258.2 | 8258.2 | 1376.37 | 19.32 | 0 |
| Linear | 3 | 7422 | 7422 | 2474 | 34.73 | 0 |
| pow | 1 | 3844 | 3844 | 3844 | 53.97 | 0 |
| speed | 1 | 2209 | 2209 | 2209 | 31.01 | 0 |
| pre | 1 | 1369 | 1369 | 1369 | 19.22 | 0.001 |
| Square | 2 | 498.2 | 498.2 | 249.1 | 3.5 | 0.061 |
| speed*speed | 1 | 316.6 | 395.7 | 395.71 | 5.56 | 0.035 |
| pre*pre | 1 | 181.6 | 181.6 | 181.95 | 2.55 | 0.134 |
| Interaction | 1 | 338 | 338 | 338 | 4.75 | 0.048 |
| pow*speed | 1 | 338 | 338 | 338 | 4.75 | 0.048 |
| Residual Error | 13 | 926 | 926 | 71.23 | | |
| Lack-of-Fit | 8 | 652.7 | 652.7 | 81.58 | 1.49 | 0.342 |
| Pure Error | 5 | 273.3 | 273.3 | 54.67 | | |
| Total | 19 | 9184.2 | | | | |

| (b) | | | | | | |
|----------------|----|---------|---------|---------|-------|-------|
| Source | DF | Seq SS | Adj SS | Adj MS | F | P |
| Regression | 5 | 61943.2 | 61943.2 | 12388.6 | 34.42 | 0 |
| Linear | 3 | 32222 | 32222 | 10740.7 | 29.84 | 0 |
| pow | 1 | 7569 | 7569 | 7569 | 21.03 | 0 |
| speed | 1 | 20164 | 20164 | 20164 | 56.03 | 0 |
| pre | 1 | 4489 | 4489 | 4489 | 12.47 | 0.003 |
| Square | 2 | 29721.2 | 29721.2 | 14860.6 | 41.29 | 0 |
| speed*speed | 1 | 28315.5 | 29669.3 | 29669.3 | 82.44 | 0 |
| pre*pre | 1 | 1405.7 | 1405.7 | 1405.7 | 3.91 | 0.068 |
| Residual Error | 14 | 5038.6 | 5038.6 | 359.9 | | |
| Lack-of-Fit | 9 | 4788.6 | 4788.6 | 532.1 | 10.64 | 0.009 |
| Pure Error | 5 | 250 | 250 | 50 | | |
| Total | 19 | 66981.8 | | | | |

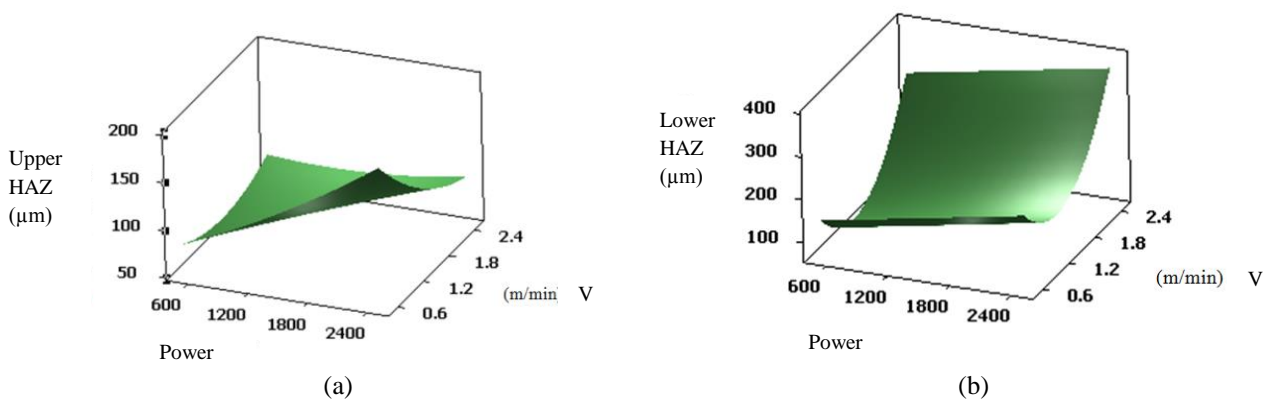


Fig. 18- The Effect of Power and Cutting Speed Parameters on (a) Depth of HAZ in the Upper One-Third of the Sheet and (b) Lower Two-Third of the Sheet in 4mm Sheet with Axillary Gas Pressure of 2.5barr

With increase in cutting speed, the depth of HAZ decreases. With increase in power in figure (19a), the depth of HAZ increases while increase in axillary gas pressure has no significant effects on the depth of HAZ. However, in (19b), there is a direct relation between gas pressure and depth of HAZ. Increase in the cutting speed decreases the depth of HAZ. In work conditions with lower axillary gas pressure, the depth of HAZ is larger which is due to the larger contact time between molten metal and the cutting edge and therefore larger heat transfer to the sample (figure 20).

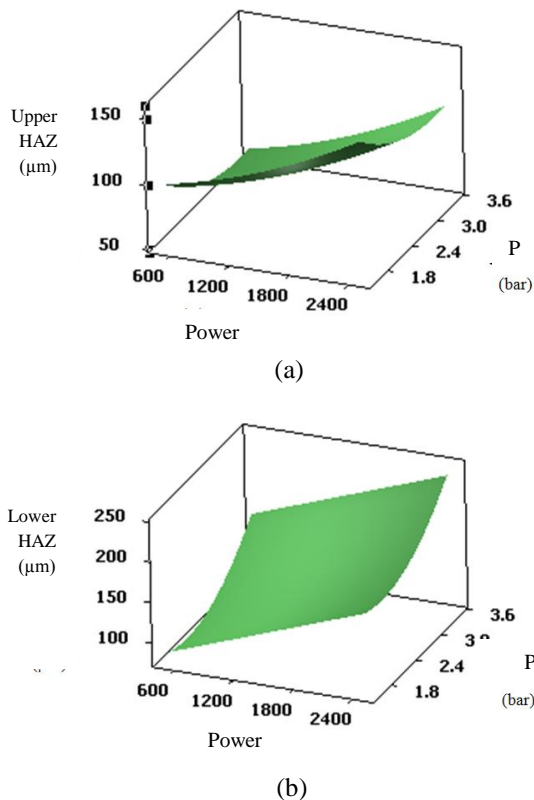


Fig. 19- The Effect of Laser Beam Power and Axillary Gas Pressure on (a) Depth of HAZ in the Upper One-Third of the Sheet and (b) Lower Two-Third of the Sheet in 4mm Sheet with Beam Movement Speed of 1.6m/min

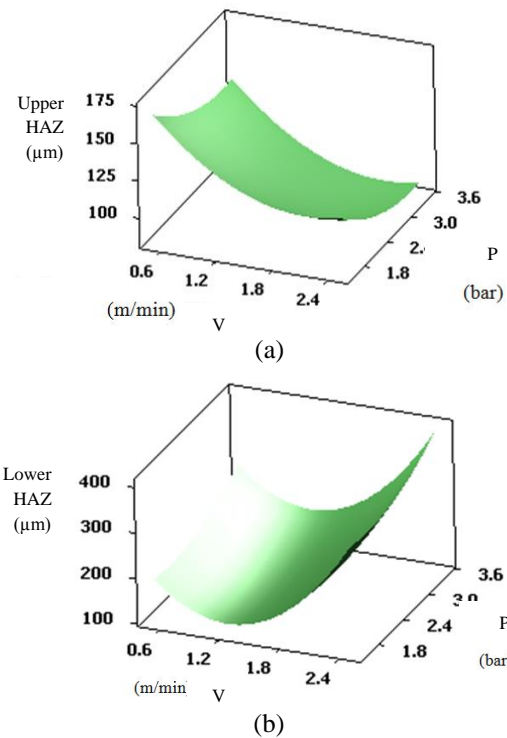


Fig. 20- The Effect of Axillary Gas Pressure and Cutting Speed Parameters on (a) Depth of HAZ in the Upper One-Third of the Sheet and (b) Lower Two-Third of the Sheet in 4mm Sheet with Beam Power of 1700W

4.4- Evaluating the Depth of Heat Affected Zone (HAZ) IN 6mm Sheets

After carrying out the experiments designed based on response surface method, the responses for Mild Steel St37 sheet with thickness of 6mm were extracted and presented in tables (10) and (11). Regression equations for evaluating the depth of heat affected zone in the upper one-third and lower two-third of the thickness of 6mm sheets are presented in (14) and (15).

$$\begin{aligned}
 \text{HAZ} - 6 = & 0.0868750 (\text{pow}) \\
 & - 225.250(\text{speed}) \\
 & - 50.0893(\text{pre}) \\
 & + 67.5714(\text{speed})^2 \\
 & + 6.89286(\text{pre})^2 \\
 & - 0.0350000(\text{pow} \\
 & \times \text{speed}) + 327.348
 \end{aligned} \quad (14)$$

$$\begin{aligned} \text{HAZ} - 6/D = & 0.0176477(\text{pow}) - \\ & 329.852(\text{speed}) - 394.670(\text{pre}) + \\ & 1.54091\text{E} - 05(\text{pow})^2 + \quad (15) \\ & 135.409(\text{speed})^2 + 85.4091(\text{pre})^2 + \\ & 732.040 \end{aligned}$$

Table 9- Experiment Design Using Response Surface Method for Mild Steel St37 Sheets with 6mm Thickness with HAZ Depth as the Output.

| power | speed | pre | D1.30 up/t=6 | D2.30 down/t=6 |
|-------|-------|-----|-----------------|-------------------|
| 1000 | 1 | 2 | 110 | 145 |
| 2000 | 1 | 2 | 150 | 190 |
| 1000 | 2 | 2 | 90 | 205 |
| 2000 | 2 | 2 | 110 | 250 |
| 1000 | 1 | 3 | 85 | 134 |
| 2000 | 1 | 3 | 125 | 225 |
| 1000 | 2 | 3 | 80 | 240 |
| 2000 | 2 | 3 | 100 | 330 |
| 500 | 1.5 | 2.5 | 80 | 100 |
| 2500 | 1.5 | 2.5 | 125 | 220 |
| 1500 | 1 | 2.5 | 130 | 210 |
| 1500 | 2.5 | 2.5 | 90 | 350 |
| 1500 | 0.5 | 1.5 | 115 | 200 |
| 1500 | 1.5 | 3.5 | 85 | 260 |
| 1500 | 1.5 | 2.5 | 88 | 160 |
| 1500 | 1.5 | 2.5 | 90 | 155 |
| 1500 | 1.5 | 2.5 | 95 | 165 |
| 1500 | 1.5 | 2.5 | 100 | 145 |
| 1500 | 1.5 | 2.5 | 85 | 135 |
| 1500 | 1.5 | 2.5 | 95 | 130 |

After determining the regression equation for the evaluation of depth of HAZ in 6mm sheets in the upper one-third and lower two-third of the thickness, the relation between various parameters is investigated. Figure (21a) shows that increase in cutting speed significantly decreases the depth of HAZ. Under work conditions with low axillary gas pressure, the depth of HAZ is a little larger which is due to longer contact time between the molten metal and cutting edge and subsequent increase in transferred heat to the sample. As can be seen in speed – pressure graph (figure 21b), increase in cutting speed and gas pressure first decreases the depth of HAZ and then significantly increases the depth of HAZ after a certain point. The depth of HAZ at the lower part of the sheet is also significantly higher than the depth of HAZ at the upper part of the sheet. This is due to larger contact time with molten metal and lower part of the sheet as a result of longer time necessary for removal of the molten metal from the lower part of the cut.

Table 10- ANOVA Results for HAZ-6 (a) HAZ in Upper One-Third of 6mm Sheet (b) HAZ in Lower Two-Third of 6mm Sheet

(a)

| Source | DF | Seq SS | Adj SS | Adj MS | F | P |
|----------------|----|---------|---------|---------|-------|-------|
| Regression | 6 | 5953.84 | 5953.84 | 992.31 | 21.91 | 0 |
| Linear | 3 | 5304.69 | 5304.69 | 1768.23 | 39.05 | 0 |
| pow | 1 | 2626.56 | 2626.56 | 2626.56 | 58 | 0 |
| speed | 1 | 1701.56 | 1701.56 | 1701.56 | 37.57 | 0 |
| pre | 1 | 976.56 | 976.56 | 976.56 | 21.56 | 0 |
| Square | 2 | 496.03 | 496.03 | 248.02 | 5.48 | 0.019 |
| speed*speed | 1 | 417.78 | 470.02 | 470.02 | 10.38 | 0.007 |
| pre*pre | 1 | 78.25 | 78.25 | 78.25 | 1.73 | 0.211 |
| Interaction | 1 | 153.12 | 153.12 | 153.12 | 3.38 | 0.089 |
| pow*speed | 1 | 153.12 | 153.12 | 153.12 | 3.38 | 0.089 |
| Residual Error | 13 | 588.71 | 588.71 | 45.29 | | |
| Lack-of-Fit | 8 | 437.87 | 437.87 | 54.73 | 1.81 | 0.265 |
| Pure Error | 5 | 150.83 | 150.83 | 30.17 | | |
| Total | 19 | 6542.55 | | | | |

(b)

| Source | DF | Seq SS | Adj SS | Adj MS | F | P |
|----------------|----|---------|---------|---------|-------|-------|
| Regression | 6 | 78839.7 | 78839.7 | 13140 | 45.42 | 0 |
| Linear | 3 | 43845.2 | 43845.2 | 14615.1 | 50.51 | 0 |
| pow | 1 | 16320.1 | 16320.1 | 16320.1 | 56.41 | 0 |
| speed | 1 | 23332.6 | 23332.6 | 23332.6 | 80.65 | 0 |
| pre | 1 | 4192.6 | 4192.6 | 4192.6 | 14.49 | 0.002 |
| Square | 3 | 34994.6 | 34994.6 | 1664.9 | 40.32 | 0 |
| pow*pow | 1 | 943.5 | 373.1 | 373.1 | 1.29 | 0.277 |
| speed*speed | 1 | 22587.9 | 28813.1 | 28813.1 | 99.59 | 0 |
| pre*pre | 1 | 11463.1 | 11463.1 | 11463.1 | 39.62 | 0 |
| Residual Error | 13 | 3761.2 | 3761.2 | 289.3 | | |
| Lack-of-Fit | 8 | 2777.9 | 2777.9 | 347.2 | 1.77 | 0.275 |
| Pure Error | 5 | 983.3 | 983.3 | 196.7 | | |
| Total | 19 | 82601 | | | | |

On the other hand, excess increase in the cutting speed prevents the complete removal of the molten metal, leading to both lower cut quality and increased depth of HAZ due to remaining molten metal in the cut. Excess increase in the axillary gas pressure also has similar effect to excess increase in cutting speed, reducing the quality of cutting edge and increasing the depth of HAZ due to increased cut width at the upper part and accumulation of molten metal at the lower part of the sheet. With increase in laser power, the depth of HAZ increases while increase in axillary gas pressure decreases the depth of HAZ. Based on the power – speed and power – pressure graphs in figure (22), it can be said that the effect of speed and pressure on the depth of HAZ is higher than the effect of laser power at the lower part of the sheet. With the increase in laser power, energy density on the surface unit increases, leading to increased temperature at the cut's location and larger depth of HAZ. The power – speed graph of figure (23) shows that, generally, increase in power increases the depth of HAZ. This effect is larger at lower cutting speeds due to increased interaction time between the beam and the sheet and thus increased heat

transfer to the sample. In lower speeds, cutting surface is also affected by the beam for a longer time, increasing the heat transfer rate and depth of HAZ. With increase in cutting speed, the depth of HAZ decreases.

Next, figures 24 to 31 are investigated which show the edge of the cut area. Comparing figures 24 and 25 shows that with increase in pressure at the lower part of the sheet, surface roughness increases and the quality of cutting edge significantly decreases. Comparing figures 24 and 26 shows that increase in laser power to higher than average values increases the surface roughness. Comparing figures 24 and 27 shows that increase in cutting speed changes the quality of cutting edge and increases the surface roughness. Comparing figures 28 and 29 shows that with the increase in pressure at the lower part of the sheet, surface roughness increases and the quality of cutting edge significantly decreases. Comparing figures 28 and 30 shows that increase in laser power to higher than average values increases the surface roughness. Comparing figures 28 and 31 shows that increase in cutting speed

changes the quality of cutting edge and increases the surface roughness.

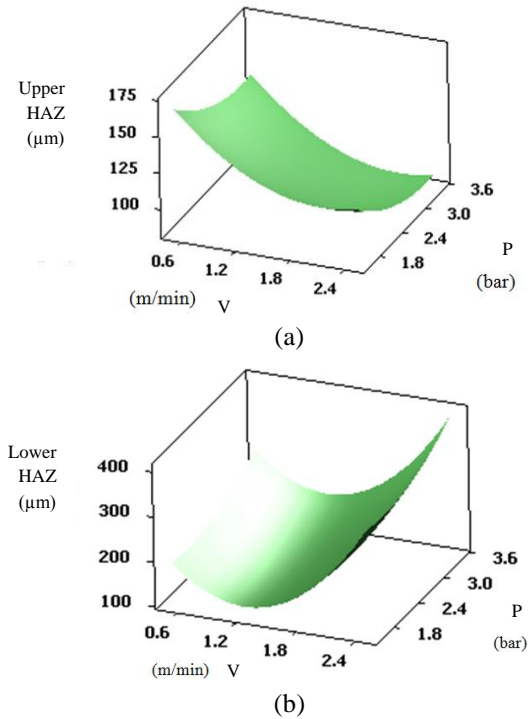


Fig. 21- Effect of Axillary Gas Pressure and Laser Beam Movement Speed Parameters on (a) Depth of HAZ in the Upper One-Third and (b) Lower Two-Third of 6mm Sheet with Power of 1700W

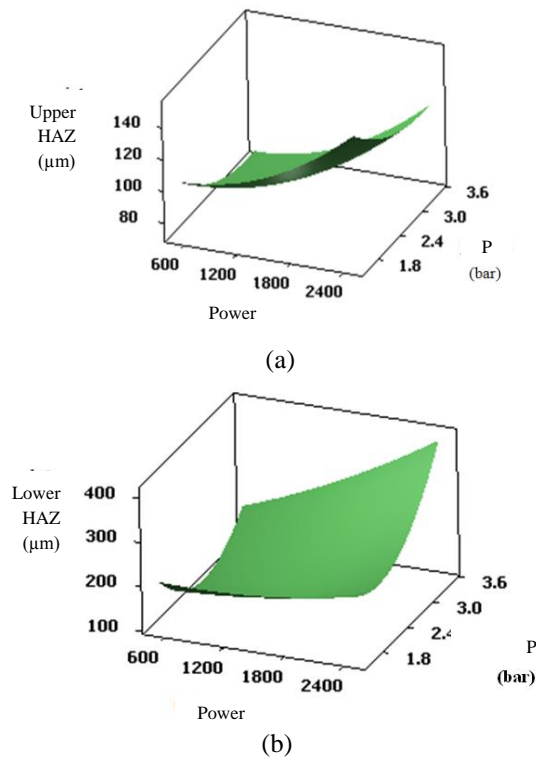


Fig. 22- Effect of Axillary Gas Pressure and Laser Power Parameters on (a) Depth of HAZ in the Upper One-Third and (b) Lower Two-Third of 6mm Sheet with Cutting Speed of 1.6m/min

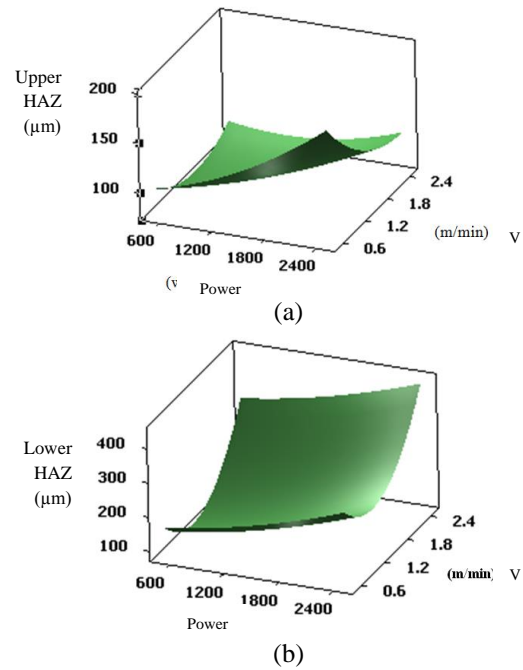


Fig. 23- Effect of Laser Beam Power and Movement Speed Parameters on (a) Depth of HAZ in the Upper One-Third and (b) Lower Two-Third of 6mm Sheet with Gas Pressure of 2.5bar

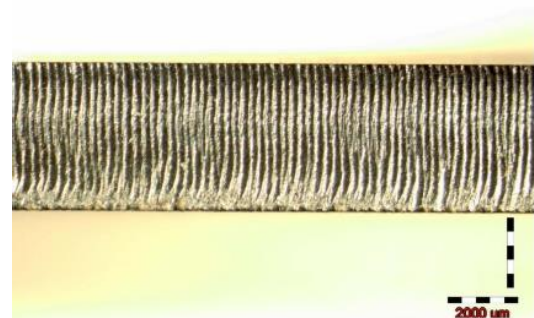


Fig. 24, Image of the Cutting Edge in 4mm Sheet Under 2.5bar Pressure, 1.5m/min Cutting Speed and Power of 2000W

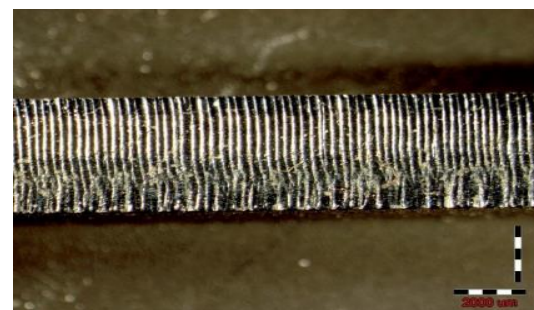


Fig. 25, Image of the Cutting Edge in 4mm Sheet under 2.5bar Pressure, 2.5m/min Cutting Speed and Power of 1500W

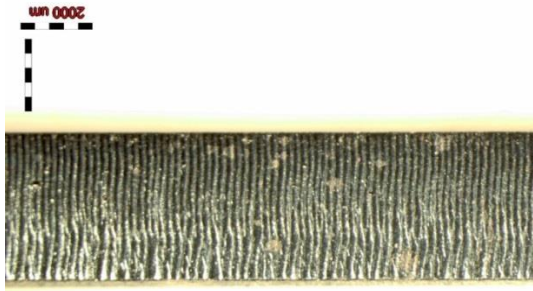


Fig. 26- Image of the Cutting Edge in 4mm Sheet under 2.5bar Pressure, 1.5m/min Cutting Speed and Power of 2000W

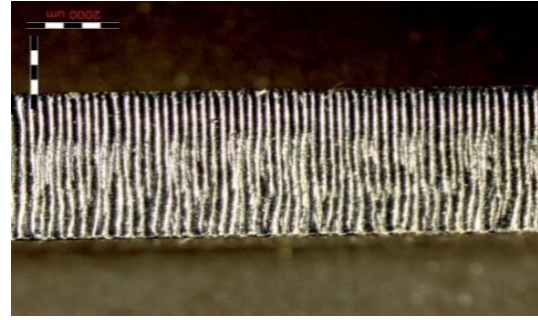


Fig. 30- Image of the Cutting Edge in 6mm Sheet under 2.5bar Pressure, 1.5m/min Cutting Speed and Power of 2000W

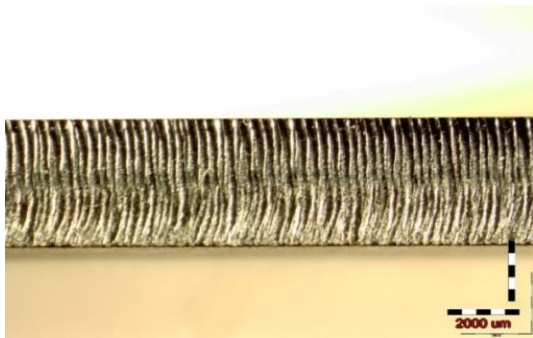


Fig. 27- Image of the Cutting Edge in 4mm Sheet under 2.5bar Pressure, 2.5m/min Cutting Speed and Power of 1500W

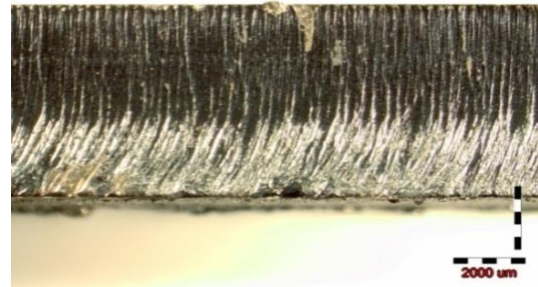


Fig. 31- Image of the Cutting Edge in 6mm Sheet under 2.5bar Pressure, 2.5m/min Cutting Speed and Power of 1500W

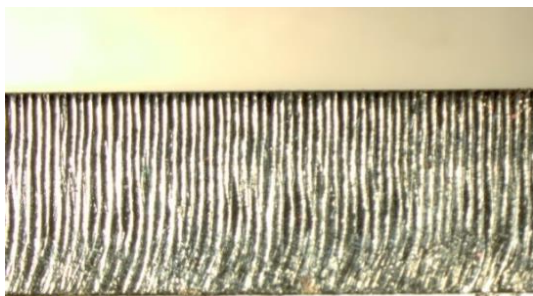


Fig. 28- Image of the Cutting Edge in 6mm Sheet under 2.5bar Pressure, 1.5m/min Cutting Speed and Power of 1500W



Fig. 29- Image of the Cutting Edge in 6mm Sheet under 3.5bar Pressure, 1.5m/min Cutting Speed and Power of 1500W

5- Conclusion

In the current study, the laser cutting process of Mild Steel St37 sheets with two thicknesses of 4 and 6 mm was investigated empirically. A finite element simulation was also carried out by considering a normal Gaussian distribution function as the source of heat flow. In order to perform the experiments, response surface method was used to determine the number of necessary experiments and the conditions of each experiment and samples were cut using laser cutting equipment with different parameters. Then, supplementary tests were carried out to determine the microstructures and surface roughness of the samples. Evaluation of the results can lead to the following conclusions:

1. The curvature of response levels confirms the suitable use of the method. Furthermore, these results show that the

ranges of process parameters are correctly selected and there is suitable optimization in the considered parameter space.

2. All three parameters of laser beam movement speed, axillary gas pressure and laser power significantly affect the output of roughness parameters (Ra, Rz) and depth of heat affected zone.

3. With increase in cutting speed at constant gas pressure, surface roughness first decreases and then increases after the speed exceeds a certain limit. Therefore, it can be concluded that the rate of heat transfer to the samples over time decreases with increase in cutting speed which reduces the available time for melting of the metal and removal of molten metal, leading to increased surface roughness. Increasing the pressure of axillary gas also first reduces the surface roughness and then significantly increases the roughness after a certain point which shows the effect of gas pressure on surface roughness (due to removal of molten metal).

4. Both parameters of power and pressure should be optimized at a suitable level. Simultaneous selection of too low or too high values for power and pressure can lead to significant increase in surface roughness.

5. In low power levels (600W), increase in speed significantly increases the surface roughness which is due to lack of sufficient temperature for melting at the cutting location. With increase in laser's power, this effect is reduced and roughness reaches its lowest level. Excess increase in power increases surface roughness which is due to lower cut quality due to excess temperature and molten metal splashing and oxidation of the metal.

6. In laser cutting process, surface roughness increases with increase in sheet's thickness. The main reason for this is divergence of the laser beam from its focal point.

7. The results also indicate similar trends in changes of Rz and Ra.

8. Furthermore, increase in power increases the depth of heat affected zone (HAZ). This effect is larger at lower cutting speeds because at lower speeds, the cut surface is exposed to the laser beam for a longer period which increases the rate of heat transfer to the sample. With increase in speed, the depth of head affected zone decreases.

9. Increase in axillary gas pressure has no significant effects on depth of heat affected zone.

10. With increase in cutting speed, the depth of heat affected zone decreases and this parameter has a significant effect on depth of HAZ. At work conditions with low axillary gas pressure, the depth of HAZ is larger because molten metal is in contact with the cut for a longer period of time which increases the rate of heat transfer to the sample.

11. Generally, increase in speed and gas pressure first decrease and then significantly increase the depth of HAZ. The size of HAZ at the lower part of the sheet is also larger compared to the upper part of the sheet. The reason is before removal of molten metal, the lower part of the sheet is exposed to higher temperatures which is due to longer contact time with molten metal. Therefore, the depth of HAZ at the lower part of the sheet is larger compared to upper part of the sheet. On the other hand, excess increase in speed of removal of molten metal prevents full

removal of the molten metal, thus reducing the quality of cutting edge and increasing the depth of HAZ.

12. Excess increase in axillary gas pressure has similar effect to excess increase in cutting speed, reducing the quality of cutting edge and increasing the depth of HAZ. This is due to increased width of the cut at the upper part of the sheet and accumulation of molten metal at lower part of the cut.

13. According to speed, power and pressure graphs, the effects of speed and pressure on the depth of HAZ at the lower part of the sheet is higher than the effect of laser power.

14. With increase in laser power, the energy density on units of surface always increases which in turn increases the temperature of the cut and depth of HAZ.

15. Comparison between finite element simulation results and experimental results shows the acceptable accuracy of numerical results for simulating heat distribution in samples.

16. The temperature counters extracted from finite element simulation method can determine the depth of the HAZ with a good estimation and have acceptable accuracy in simulating the depth of HAZ and upper and lower part of the sheet.

17. Finally, finite element simulation when the heat released due to exothermic oxidation reaction of steel is considered, has acceptable accuracy in simulating the laser cutting process. As a result, this method can be used for parametric investigation of laser cutting process in order to save time and money (before start of the actual experiments).

References

- [1] Poprawe, R., Tailored Light. Springer, (2012).
- [2] Chen, X., Li, T., Zhai, K., Zhou, M., “Using orthogonal experimental method optimizing surface quality of CO₂ laser cutting process for PMMA microchannels”, The International Journal of Advanced Manufacturing Technology, Vol. 88, No. 9-12, pp. 2727-2733, (2017).
- [3] Shin, J.S., Oh, S.Y., Park, H., Chung C.M., Seon, S., Kim, T.S., Lee, L., Choi B.S., Moon, J.K., “High-speed fiber laser cutting of thick stainless steel for dismantling tasks”, Optics & Laser Technology, Vol. 94; pp. 244-247, (2017).
- [4] Rodrigues, G.C. Duflou J.R., “Opportunities in laser cutting with direct diode laser configurations”, CIRP Annals-Manufacturing Technology, (2017).
- [5] Niziev, V. and A. Nesterov, “Influence of beam polarization on laser cutting efficiency”, Journal of Physics D: Applied Physics, Vol. 32, No.13, p. 1455, (1999).
- [6] Chen, K., Lawrence Yao Y., Modi V., “Numerical simulation of oxidation effects in the laser cutting process”, The International Journal of Advanced Manufacturing Technology, Vol. 15, No.11, pp. 835-842, (1999).
- [7] Galantucci, L., Giusti F., “Excimer laser cutting: experimental characterization and 3D numerical modelling for polyester resins”, CIRP Annals-Manufacturing Technology, Vol. 47, No.1, pp. 141-144, (1998).
- [8] Li, K., Sheng P., “Plane stress model for fracture of ceramics during laser cutting”, International Journal of Machine Tools and Manufacture, Vol. 35, No.11, pp. 1493-1506, (1995).
- [9] Kaplan, A.F., “An analytical model of metal cutting with a laser beam”, Journal of applied physics, Vol. 79, No.5, pp. 2198-2208, (1996).
- [10] Schulz, W., Becker, D., Franke, J., Kemmerling R., Herziger G., “Heat conduction losses in laser cutting of metals”, Journal of Physics D: Applied Physics, Vol. 26, No.9, p. 1357, (1993).
- [11] Wee, L.M., Li L., “An analytical model for striation formation in laser cutting”, Applied Surface Science, Vol. 247, No.1, pp. 277-284, (2005).
- [12] Chen, S.-L., “The effects of gas composition on the CO₂ laser cutting of mild steel”, Journal of

materials processing technology, Vol. 73, No.1, pp. 147-159, (1998).

[13] Karatas, C., Keles, O., Uslan I., Usta Y., “Laser cutting of steel sheets: Influence of workpiece thickness and beam waist position on kerf size and stria formation”, *Journal of Materials Processing Technology*, Vol. 172, No.1, pp. 22-29, (2006).

[14] Wandera, C., Kujanpaa, V., “Characterization of the melt removal rate in laser cutting of thick-section stainless steel”, *Journal of Laser Applications*, Vol. 22, No.2, pp. 62-70, (2010)

[15] Eltawahni, H.A., Hagino, M., Benyounis, K.Y., Inoue, T., Olabic, A.G., “Effect of CO2 laser cutting process parameters on edge quality and operating cost of AISI316L”, *Optics & Laser Technology*, Vol. 44, No.4, pp 1068-1082, (2012).

[16] Rao, S., Sethi, A., Kumar Das, A., Mandal, N., Kiran, P., Ghosh, R., Dixit, A. R., Mandal, A., “Fiber laser cutting of CFRP composites and process optimization through response surface methodology”, *Materials and Manufacturing Processes*, pp. 1-10, (2017).

[17] Madić, M., Antucheviciene., J., Radovanović, . M., Petković, D., “Determination of laser cutting process conditions using the preference selection index method”, *Optics & Laser Technology*, Vol. 89: pp. 214-220, (2016).

[18] Amjadi, M. S. , Foroozmehr, E. ,Badrossamay, M., “Study of heat-affected zone (HAZ) caused by cutting of Thin Ti-CP Sheet via CW CO2 Laser”, *Modares Mechanical Engineering*, Vol. 17, No. 5, pp. 253-259, (2017) (in Persian)

[19] Moradi, M., Ghoreishi, M., “Influences of laser welding parameters on the geometric profile of NI-base superalloy Rene 80 weld-bead”, *The International Journal of Advanced Manufacturing Technology*, Vol. 55, No. 1-4, pp. 205-215, (2011).

[20] Moradi, M., Mehrabi, O. , Azdast, T. , Benyounis, Kh. Y. , ”The effect of low power co2 laser cutting process parameters on polycarbonate cut quality produced by injection molding”, *Modares Mechanical Engineering*, Vol. 17, No. 2, pp. 93-100, (2017) (in Persian)

[21] DRÁBEK, M., Měření drsnosti řezných hran při laserovém dělení kovů. Brno Bakalářská práce. Vysoké učení technické v Brně, Fakulta strojního inženýrství, Ústav strojírenské technologie, 42 s., 1 příloha. Vedoucí práce RNDr. Libor Mrňa, Ph.D, (2012).

[22] Zhang, L., Michaleris, P., “Investigation of Lagrangian and Eulerian finite element methods for modeling the laser forming process”, *Finite elements in analysis and design*, Vol. 40, No. 4, pp. 383-405, (2004).

[23] Bergman, T. L., Lavine, A.S., Incropera, F.P., DeWitt, D.P., “Incropera, Fundamentals of heat and mass transfer”, John Wiley & Sons, (2011).

[24] Kothandaraman, C., *Fundamentals of heat and mass transfer*. New Age International, (2006).

[25] Ion, J., *Laser processing of engineering materials: principles, procedure and industrial application*. 2005: Butterworth-Heinemann, (2005).

